ADVANCED MATERIALS INTERFACES
www.advmatinterfaces.de

The Growth of Metal–Organic Framework Films on Calcium Fluoride and Their Interaction With Reactive Molecules

*Laurens D. B. Mandemaker, Christia Jabbour, Nikolaos Nikolopoulos, Joren M. Dorresteijn, Miguel Rivera-Torrente, and Bert M. Weckhuysen**

Spectroscopy on metal–organic framework (MOF) films and the molecular phenomena associated to them is mostly limited to grazing incidence methods. To allow for transmission-based characterization and highlight the applicability of MOFs on transparent substrates, UiO-67, UU-1, and ZIF-8 MOFs are synthesized on CaF_2 windows. It is revealed that the growth of the UiO-67 MOF follows a Volmer–Weber mechanism using scanning electron microscopy (SEM). This growth is assisted by growing seeds in solution, which anchor on the film and become part of the intergrown film itself. UU-1, a copper-based MOF, is formed after spin coating the Cu-BTC precursors, showing its characteristic fiber-like morphology and resulting inter-fiber macroporosity. ZIF-8 is formed using a "flash"-synthesis, and it is shown that this approach resembles a Volmer–Weber growth mode as well. Last, CO probe molecule adsorption FT-IR spectroscopy is utilized to study the effect of methanol exposure. UiO-67 becomes inaccessible toward CO, due to the formation of methoxy species, whereas UU-1 undergoes a topotactic transformation to HKUST-1. ZIF-8 is the most stable as methanol only removes impurities from the framework. This approach opens the venue for other film materials to be studied in situ synthesis, sorption, or catalysis using transmission-based spectroscopy.

1. Introduction

Metal–organic frameworks (MOFs) are a class of porous crystalline materials that are gaining a lot of attention due to their ease in tunability of both structure and composition.[1] Within this context, attention is going toward MOF thin films, which are gaining even bigger interest nowadays because they broaden the application window of MOFs, such as in the use of monolithic MOF membranes in gas permeation experiments, electrochemical energy storage or catalytically active coatings.[2–4] Being able to control the morphology is very important to fine-tune the material toward specific applications. Some reported work already highlights the great advantage of, for example, monolithic-catalyst membranes over their powder form.[5]

Typically, MOF (thin) films are anchored on a supportive substrate to yield a surface-anchored MOF (SURMOF) instead of a self-supportive membrane. The type of substrate has a strong influence on the resulting morphology and defective nature of the SURMOF.[3] Whilst some substrates (e.g., metal oxides) can act as anchor points to grow the MOF material from the solution, other substrates require a pretreatment step with an organic compound to bind the initial nuclei to the surface. These compounds are often applied as self-assembled monolayers (SAMs). By varying the anchoring groups of the SAM, different orientational growth of the same MOF can be observed.[6,7]

MOF thin films can be prepared by a wide range of synthesis methods and conceptual approaches.[3,8,9] The most straightforward method involves a direct synthesis (DS) through a solvothermal process, where the substrate is incubated along with the reaction mixture.[10] Spin coating techniques (SCT),[11,12] dip coating and layer-by-layer (LbL), or liquid epitaxy deposition, are indirect synthesis techniques that require multiple repetitive steps, the so-called cycles.[13–15] The latter method has been explored to produce SURMOFs with low surface roughness and a low amount of defects. However, every MOF requires a specific set of synthesis parameters to result in homogeneous closed films of crystalline SURMOFs due to the specific chemistry of each ligand-metal–solvent–substrate combination. Some MOFs can grow at room temperature, such as HKUST-1, while

L. D. B. Mandemaker, C. Jabbour, N. Nikolopoulos, J. M. Dorresteijn, M. Rivera-Torrente, B. M. Weckhuysen
Inorganic Chemistry and Catalysis Group
Debye Institute for Nanomaterials Science
Utrecht University
Universiteitsweg 99, Utrecht 3584CG, The Netherlands
E-mail: b.m.weckhuysen@uu.nl

The ORCID identification number(s) for the author(s) of this article can be found under https://doi.org/10.1002/admi.202201753.

DOI: 10.1002/admi.202201753

other framework structures require high temperatures to crystalize, as is the case, for example, with UiO-67.[16,17] Therefore, a LbL technique might not always be the most suitable choice. Hence, our efforts were directed toward studying a set of relevant topologies with different features by means of depositing them on calcium fluoride (CaF_2) windows using three different techniques which suit the corresponding MOF.

In one of our earlier works, we demonstrated the growth of Cu-BTC MOF material HKUST-1 as a SURMOF on such windows, which used a SAM of 4-(trifluoromethyl)benzoic acid to create a layer of terminated carboxylic acid groups, which are often used to anchor MOFs.[18] These windows are optically transparent for light in the UV–vis and IR range, which is highly beneficial when characterizing and quantifying chemical processes using transmission-based spectroscopic tools. In this work, we demonstrate the wide applicability of these windows for spectroscopic analysis by introducing three different MOFs (i.e., UiO-67, UU-1, and ZIF-8) on CaF_2, all with completely different chemical compositions and morphologies, as is schematically shown and highlighted with atomic force microscopy (AFM) in **Figure 1**. First of all, every single MOF contains a different metal node (Zr, Cu, Zn) which is relevant to the initial binding of the "first metal layer" to the acid-functionalized CaF_2 window. Second, all MOFs used have different crystal structures, leading to varying stability and morphology of the structure, which might affect the binding affinity on the functionalized windows. Last, they are all purposely generated using varying synthesis procedures to test the survivability of the functionalized CaF_2 windows in higher temperatures during a solvothermal synthesis (UiO-67) or during consecutive exposure to reagent solutions which are then evaporated, either due to spin coating (UU-1) or rapid heating (ZIF-8).

To assess the formation of these MOFs on the CaF_2 windows, we first use scanning electron microscopy (SEM) to look at the MOF formation under varying synthesis concentrations and temperatures for the different MOFs. Then, we explain the growth mechanism of UiO-67 and ZIF-8 films under the conditions found to be optimal and, complemented by X-ray diffraction (XRD), confirming the formation of the new UU-1 MOF. Last, CO probe molecule adsorption FT-IR spectroscopy is used to study the MOF films and their active sides before and after methanol exposure, which is possible due to the transparent nature of the anchoring CaF_2 substrate.

2. Results and Discussion

2.1. Solvothermal Synthesis of UiO-67 on CaF_2

UiO-67 is a zirconium-based MOF made of $Zr_6(OH)_4O_4$ clusters that are linked to biphenyl dicarboxylate (H_2bpdc), which acts as a bridging ligand. UiO-67 films were synthesized using a DS approach, partly based on the procedure from Øien-Ødegaard et al.[17] The precursors were dissolved in DMF before the 4-(trifluoromethyl)benzoic acid functionalized CaF_2 was added.[18] To study the influence of both the reagent concentration and the reaction temperature, scanning electron microscopy (SEM) images were obtained on the windows after synthesis at

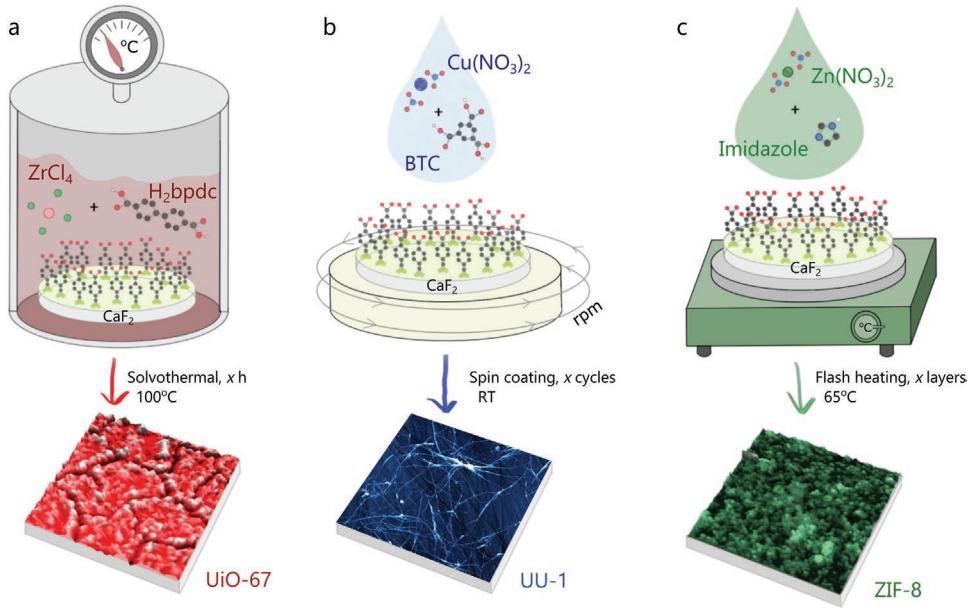

Figure 1. Schematic approach for the formation of three metal–organic framework (MOF) films, namely a) UiO-67, b) UU-1 (vide infra), and c) ZIF-8, on functionalized UV–vis and IR-transparent CaF_2 windows. While the UiO-67 film is synthesized using a solvothermal method, in which the linker and metal cluster react in one-pot with the substrate, both UU-1 and ZIF-8 are formed by depositing a number of cycles, or layers, either by spin coating or drop casting while at high temperature ("flash heating"), respectively. The atomic force micrographs reveal the distinct morphologies for the MOF films, showing the formation of a cracked closed film (UiO-67, 9 h), long thin nanowebs (UU-1, 150 cycles), and a closed smooth film (ZIF-8, six cycles). All AFM images share the same *xyz* dimensions.

80 °C, 100 °C, and 120 °C (with 43 mM precursor concentration) and at concentrations of 4.3, 43, and 430 mM linker and metal nodes (at 100 °C), all for 5 h, as shown in Figure S1, Supporting Information. Both the coverage and particle size seemed to be influenced significantly, which is also represented in the particle size distributions shown in Figure S2, Supporting Information. A better coverage was obtained for the sample that was synthesised at 100 °C, versus that synthesized at 80 °C. This was due to the fact that a denser layer seemed to be formed at 100 °C, on which octahedral features were more pronounced within the merged film. In addition, individual, larger octahedral particles were found (vide infra). Last, the MOF film synthesized at 120 °C had a very low coverage. A few dense, thick film-like regions were found with many large particles (Figure S1e-top, Supporting Information). However, the majority of the surface was practically empty except for some isolated, smaller, UiO-67. The higher temperature during the solvothermal synthesis was known to stimulate the formation of MOF crystals but we assume that the SAM must be desorbed from the CaF_2 window, resulting in the lower coverage of MOF on the surface. Hence, for the remainder of this work, UiO-67 MOFs will be synthesized with a precursor concentration of 43 mM and at 100 °C synthesis temperature. An X-ray diffractogram (XRD) of a typical sample (9 h synthesis time), confirming the formation of the oriented crystal structure, is shown in Figure S3, Supporting Information, highlighting the (111), (200), and (220) characteristic UiO-67 reflections.

Using these synthesis conditions, SEM images were obtained, as displayed in **Figure 2**, for different synthesis times, accompanied by particle size distributions of the crystallites "on" the surface (often showing higher intensity in the SEM image, resulting in "white" particles). SEM images show both a layer of material, which grows thicker over time with an associated increase of the amount and size of cracks, attributed to capillary phenomena during the drying process, and the many crystallites which share their size-dependence on synthesis time.[19] Therefore, it seems reasonable that the UiO-67 growth follows a Stranski–Krastanov growth mechanism, in which layer formation is primarily preferred until a critical thickness is reached, after which crystallites will form, grow, and occupy the surface.[20] The growth of the crystallites, clearly shown in the particle size distributions, follows this trend. However, as is

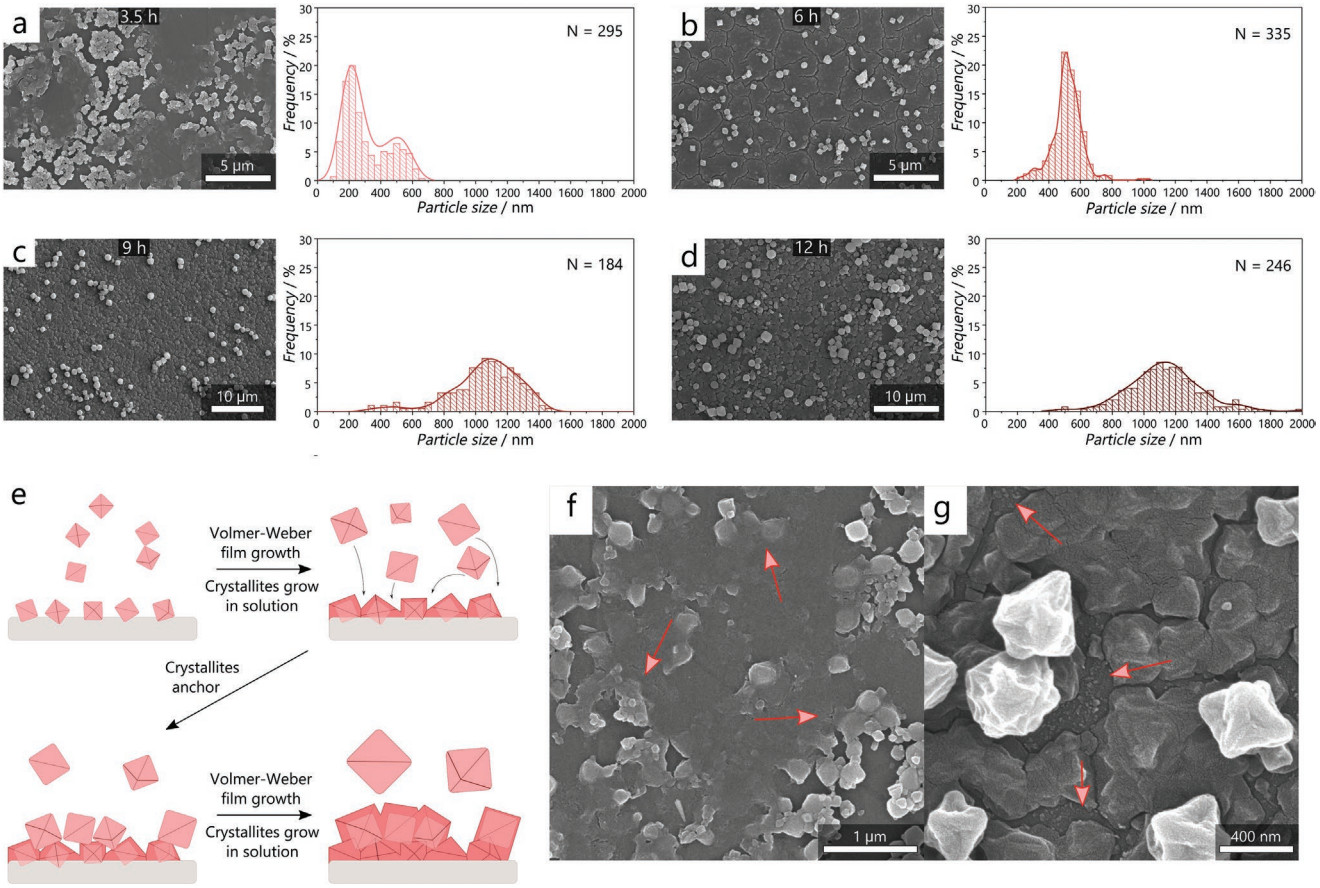

Figure 2. Scanning electron microscopy (SEM) micrographs of UiO-67 films after a) 3.5, b) 6, c) 9, and d) 12 h of synthesis time, accompanied by particle size distributions of all crystallites (white in the SEM micrographs) found in/on the surface. The particles become larger over time and additionally they seem to become part of the MOF layer itself, as is visible at 3.5 h. e) Schematic representation of the growth observed for the UiO-67 MOF film on the functionalized CaF_2 in the precursor solution. In parallel, Volmer–Weber growth forms the film, as is pointed out in the f) SEM image for the MOF synthesized for 3.5 h, while increasingly larger crystallites from the solution anchor on the surface. As these crystallites are then also intergrown to become part of the MOF film, different layers can be observed with SEM as highlighted for the sample synthesized for g) 6 h. The top layer consists of clear, larger intergrown crystallites while the lower layer contains a similar morphology but with smaller crystallite sizes.

already seen at short synthesis times (3.5 h, Figure 2a), some of these crystallites seem to be merged into the layer. In fact, the layer itself clearly shows morphological contrasts similar to the crystallites. Where 3.5 h synthesis time results in a bimodal distribution (200 and 520 nm) of crystallite sizes, we see that after 6 h, the smaller particles are completely intergrown to form a closed layer after 6 h. Film formation follows therefore not a Stranski–Krastanov but a Volmer–Weber type of growth, to the best of our knowledge not reported before for UiO-67 thin films but not uncommon for other MOFs.[10,21,22] When the crystallites expand and merge into a film (Figure 2a,b and additionally seen for 3.5 h in Figure 2g, red arrows), crystallites in the solution are growing in parallel and will anchor on the surface (as seen for 6, 9, and 12 h). These larger crystallites then undergo similar Volmer–Weber growth, creating a dense closed film. These steps are continuously happening, which leads to a MOF film with several layers of varying intergrown crystallites, or seeds, all in a one-pot approach.

This is confirmed in Figure 2g, for a synthesis time of 6 h, in which the top layer shows larger crystallites and morphological features visible in the layer. Furthermore, marked by the red arrows, the lower layer is still visible, showing similar intergrown crystallites but smaller. To conclude, this would mean the UiO-67 formed using this direct synthesis follows a Volmer–Weber type of growth, which is mediated by (increasingly larger) crystallites from solution, which is also in line with the shown particle size distributions from Figure 2.

2.2. Spin Coating Synthesis of UU-1 on CaF_2

The $Cu(BTC)(H_2O)_3$ crystal structure can be found as an alternative product when using HKUST-1 precursors at special synthesis conditions.[11] However, the resulting structure is fundamentally different from HKUST-1 in terms of morphology, porosity, and accessible active sites. This coordination polymer was first hinted at by Gascon et al., who denoted the formed material as "tagliatelle-like" structures,[23] explaining the crystal structure by the findings of Pech and Pickardt in 1988.[24] They used the "1D crystals" as an intermediate step to form HKUST-1 crystals on alumina but did not further exploit the coordination structure itself. In earlier work from our group, we investigated these structures and their properties as they were formed due to rapid solvent evaporation in a spin coating procedure, and we named the structures "nanowebs" as they were overlapping fibers anchored on the substrates used, forming a web-like morphology (here also shown in Figure 1).[11] Using X-ray photoelectron spectroscopy (XPS), it was found that the webs had high relative Cu^{2+} amounts compared to the more common HKUST-1, which often exhibits defective Cu^{+} species. However, the total amount of Cu was found to be lower. Furthermore, the fibers consisted of a dense structure and a large amount of carboxylic acid groups from the uncoordinated BTC-linkers. Ahmed et al. demonstrated that these structures (termed "swordlike Cu-BTC" in their work) could be synthesized using a new acousto-microfluidic method, which similarly came down to the fast evaporation of solvents, and the Cu species were found dominantly on the surface.[25]

They performed an elegant single-crystal XRD analysis with Rietveld refinement on the crystals synthesized using different conditions, which revealed crystal planes also found (but earlier unassigned[11]) in the nanowebs reported XRD diffractograms, that is, (020), (121), (131), (140), and other undefined reflections. Although small differences may be present, this could be explained by the fact that we have surface-mounted webs in larger quantity compared to the single crystals, possibly showing preferential orientation as can also be the case, for example, with HKUST-1. Nevertheless, the utilized and explained synthesis mechanism and resulting characterization show that the "nanowebs," "tagliatelle-like" structure, and "sword-like crystals" are the same coordination polymer. In the following sections, we will refer to this material as UU-1 (Utrecht University–1).

UU-1 was synthesized using optimized conditions based on an earlier work.[11] Therein, the reagent concentration was varied similar to as done within this work, and it was found that a precursor concentration of 10 mM is optimal as lower concentrations (1 mM) yielded low surface coverage, and higher concentrations (100 mM) led to CuO impurities within the web-like structure. Varying the temperature is impossible as the utilized set-up is unable to heat during spin coating but to test the effect of solvent evaporation speed, the rotation speed and solvent were varied. Based on these findings, we here coated the functionalized CaF_2 with 200 deposition cycles at each side, spun at 5000 rpm with 10 mM precursor concentration, resulting in dense, compact webs, as seen in **Figure 3**a,b. The fibers were known to consist of a high density and contained hardly any porosity themselves. However, macropores can be found in between the different fibers as becomes clear in the SEM images of the FIB sliced samples in Figure 3c,d. The pores were measured in a horizontal and vertical direction (twice per pore) and plotted in the "pore size distribution" in Figure 3e. Macropores between 150 and 600 nm were found. Figure 3f shows the XRD diffractogram of the UU-1 which, like discussed before, displays the (020), (121), (131), and (140) reflections,[25] together with two unassigned peaks at 12° and 15° found for the nanowebs before.[11] This pattern represents the $Cu(BTC)(H_2O)_3$ crystal structure.[24]

2.3. Flash Synthesis of ZIF-8 on CaF_2

Zeolitic imidazole frameworks (ZIFs) are a special class of MOFs as the imidazole linker connects the metal clusters to form zeolite-like structures.[26] ZIFs are generally more thermally robust and have smaller pore sizes than other MOFs. In particular, ZIF-8 is known for its potential separation qualities for H_2, CO_2, methane, and small olefins, and thermal stability up to 450 °C.[27] Furthermore, it is often reported to be a "hydrophobic" material, rather binding non-polar species than, for example water; although, there are contradictory results on this.[28–34] Nevertheless, it still steadily degrades in water.[30] ZIF-8 films were synthesized based on the work of Begum et al., wherein monolithic UiO-66-NH_2 films were generated with a "flash" approach.[35] In this work, the precursor solutions of the metal and linker are mixed and then dropped onto the functionalized CaF_2 which is constantly heated at

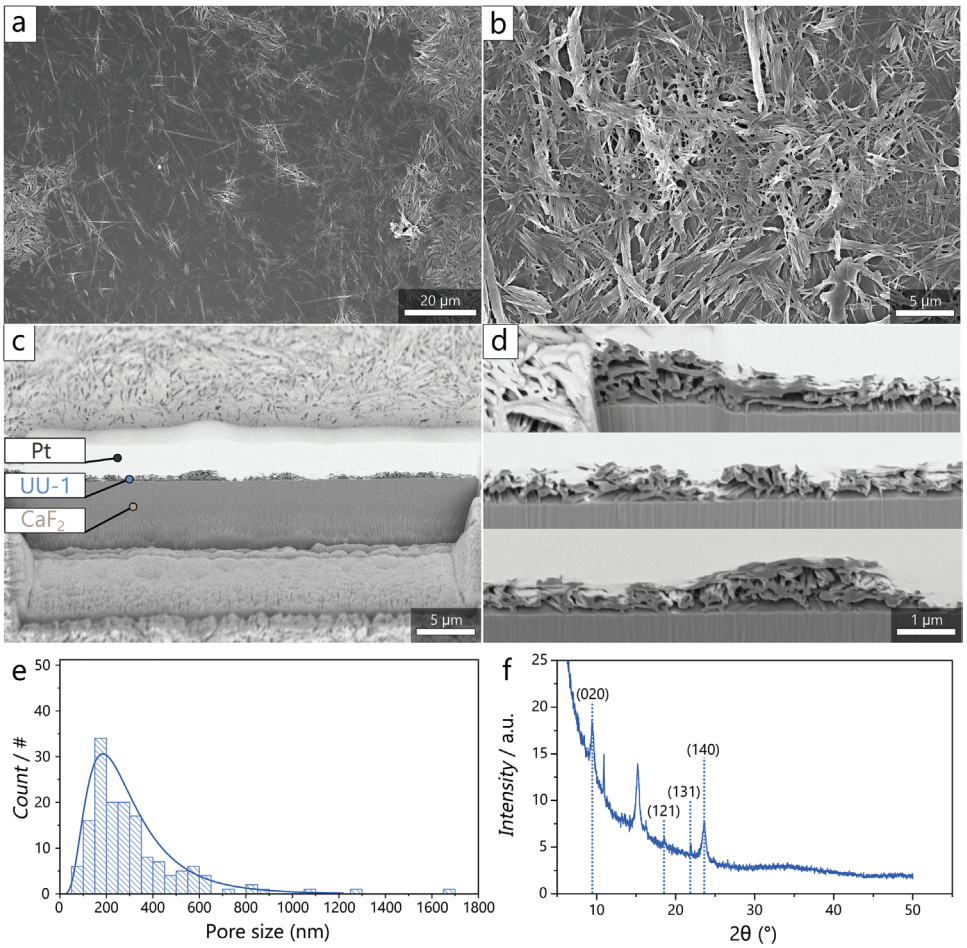

Figure 3. a) Scanning electron microscopy (SEM) images of the proposed UU-1 web-like structure covering the CaF_2 surface and b) a zoom-in showing the individual overlapping and interwoven fibers. A focused ion beam (FIB) was used to make a cross-section cut in the sample and c) SEM images show the UU-1 on the CaF_2 substrate, coated by the deposited Pt layer. d) Three further zoom-ins reveal a large amount of inter-fiber pores in the UU-1 structure. e) A distribution of the pore sizes found from FIB-SEM within the UU-1 material. f) X-ray diffraction (XRD) reveals the $Cu(BTC)(H_2O)_3$ lattice for the UU-1 fibers.

the appropriate synthesis temperature. When the mixture is dropped on the substrate, fast ("flash") evaporation of the liquid occurs, resulting in precipitated ZIF-8 film as represented in Figure 1. The "flash" synthesis is in theory a mix between the direct synthesis applied to form UiO-67 in this work and the spin-coating technique applied to form the UU-1 MOF films, with the essential benefit that all the materials dropped onto the surface are used (instead of spinning the majority away) and the reaction temperature can easily be tuned. However, this technique was not found very suitable for the UU-1 MOF as the evaporation of the liquid was too slow (with water) and the resulting high concentrations of precursor are known to yield impure UU-1.[11] Furthermore, a downside to this technique is the possible "coffee-stain" effect in which larger agglomerates of crystallites will be found on the edge area of our round CaF_2 windows (examples are shown in Figure S4a, Supporting Information).[36]

Nevertheless, ZIF-8 was synthesized using different concentrations of precursors (4, 40, and 400 mM zinc nitrate hexahydrate with 16, 160, and 1600 mM 2-methylimidazole, respectively) and different temperatures (45 °C, 65 °C, and 85 °C), all with five deposition cycles, and the resulting materials were assessed using SEM as shown in Figure S5, Supporting Information. The coverage of the material on the substrate was better than for the UiO-67 synthesized at higher temperatures, in line with the temperature-dependent desorption of the SAM from the CaF_2 when doing the synthesis in heated solvents. As becomes clear from the corresponding particle size distributions shown in Figure S6, Supporting Information, the particles seem to be unaffected for the lower concentration (Figure S6a, Supporting Information) or lower temperature (Figure S6d, Supporting Information). Nevertheless, the synthesis at 65 °C seems to yield a "closed" layer of material instead of individual particles. At higher concentrations, the particle size has increased significantly, the cubic shape of the particles is lost, and larger hexagonal crystals (Figure S5c, green arrows, Supporting Information) are found, indicating Wurtzite ZnO impurities. At higher temperatures, the coverage is lower yet the particles are identical as for the other temperatures. Instead of the desorption of the SAM, we assume here that the extremely rapid evaporation of the methanol solvent due to the high temperature does not facilitate

enough time for the ZIF-8 material to properly bind and form on the surface; hence, the lower coverage. Thus, we will use the concentration factor 1 and 65 °C synthesis temperature to synthesize ZIF-8 for the remainder of this work.

To confirm that this material is indeed ZIF-8, a sample with six deposition cycles was measured using X-ray diffraction, and the diffractogram is shown in Figure S4b, Supporting Information, which reveals the expected ZIF-8 (011), (002), (112), and (222) reflections. The morphology and thickness of the film could be controlled by increasing the number of deposition cycles. **Figure 4** shows SEM images taken on ZIF-8/CaF_2 samples for one to six subsequent cycles. On first sight, the formed material looks similar to other reported ZIF-8 films measured with electron microscopy.[37] Again, it should be noted that our windows indeed contained grains and "chunks" of agglomerated ZIF-8 crystallites were mostly on the edge, and increased thicknesses were found even after one deposition cycle on the edge of the windows. Hence, the SEM images shown in Figure 4a–d were taken on ZIF-8 found in the inner middle area, which is also the area that will represent the transmission-based FT-IR spectroscopy measurements (vide infra) the most. As can be seen after one deposition cycle, small individual islands of ZIF-8 are formed on the CaF_2 window. After another deposition cycle, these islands seem to be mostly merged; although, certain cracks are still visible. Another deposition cycle then shows a fully closed layer of ZIF-8 with larger grains growing in height. Finally, after six deposition cycles, it is shown that the material has a large amount of such higher features which dominate the morphology. As the initial growth at the first deposition cycles demonstrate that the ZIF-8 material starts with well-defined islands which later merge together into a film, while for further stages larger dominating features grow higher, this points toward- the Volmer–Weber growth mode for this substrate-film combination.

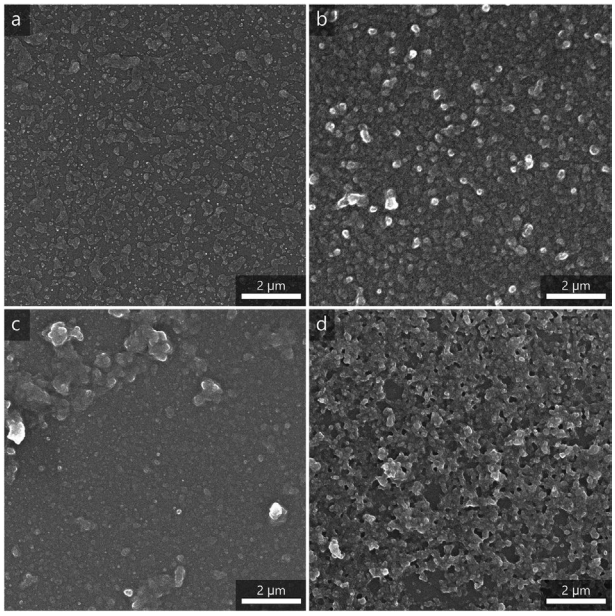

Figure 4. Scanning electron microscopy (SEM) images of ZIF-8 synthesized with a) one, b) two, c) three, and d) six deposition cycles. After the first cycle, separate islands of ZIF-8 are found. However, after two cycles, these islands are mostly connected and from three cycles onward, the film seems closed with additional material on top for more cycles.

2.4. Spectroscopic Characterization of UiO-67, UU-1, and ZIF-8

For the remainder of this work, UiO-67 was standard synthesized for 9 h, UU-1 with 400 cycles, and ZIF-8 with 6 cycles. UV–vis spectra of the MOFs were recorded in transmission mode as shown in Figure S7, Supporting Information. The observed π–π^* transitions for UiO-67 and ZIF-8, located at around 300 nm and 210 nm, respectively, are characteristic for these specific MOFs as reported before in literature.[38–41] The UU-1 shows a π–π^* band located around 220 nm due to the presence of the BTC linker. A shoulder can be observed around 300 nm, which is reported to originate from a ligand-to-metal charge transfer (LMCT) transition from oxygen atoms to the Cu ion in a HKUST-1 MOF. However, the band normally expected for HKUST-1, representing a d—d transition of the coordinating Cu^{2+} species in the spectral range of 500–1000 nm is not present for UU-1. The films are additionally rather white instead of blue, which we believe is due to the lower absolute amount of Cu^{2+} species present as compared to typical HKUST-1.[11]

2.5. Interaction With Carbon Monoxide

As MOFs are built up from a variety of metal ions, which may behave as Lewis acid sites (LAS), and organic linkers which contain hydroxyls and other typical Brønsted acid sites (BAS), IR spectroscopy during the adsorption of probe molecules, such as CO, NO, CD_3CN, CO_2, and pyridine, can provide important information on the surface hydroxyl groups, the types of acids in the material, the acid strength, and their behavior in the conversion of such molecules.[42,43] In what follows, we will first discuss the interaction of the MOF thin films with CO, while the next part will focus on the interaction with methanol as reactive molecule.

Figure 5a shows the UiO-67 film, synthesized for 9 h, during the adsorption of CO at −188 °C. The spectra are divided into the −H stretching region (left), to give information on BAS-like hydroxyls, and the C=O region additionally reveals CO adducts on LAS-like metal nanoparticles.[42] The OH region shows a major band at 3675 cm^{-1} before dosing CO, which is attributed to the ν_{OH} of unbound μ_3 hydroxyls.[44,45] As CO is dosed, the intensity of this absorption band (eventually) decreases, while the intensities of the two other absorption bands increase. The broader absorption band around 3600 cm^{-1} is due to the ν_{OH} of bound μ_3 hydroxyls: the bathochromic shift of these hydroxyl groups represents their acidic strength. This shift found for our UiO-67 MOF, $\Delta\nu$(OH) = –76 cm^{-1} (3674 to 3598 cm^{-1}), is similar as reported before for UiO-66 MOFs.[45] The C=O stretching area also reveals typical bands for this MOF as the intensities of three bands increase upon CO dosing. The sharp peak around 2150 cm^{-1} is the C=O stretch of CO adsorbed on the hydroxyl groups discussed above. It is reported that the broader band around 2130 cm^{-1} is also from the interaction of CO with these specific groups, only here, the CO is adsorbed onto the hydroxyl through the oxygen. The undefined band contribution

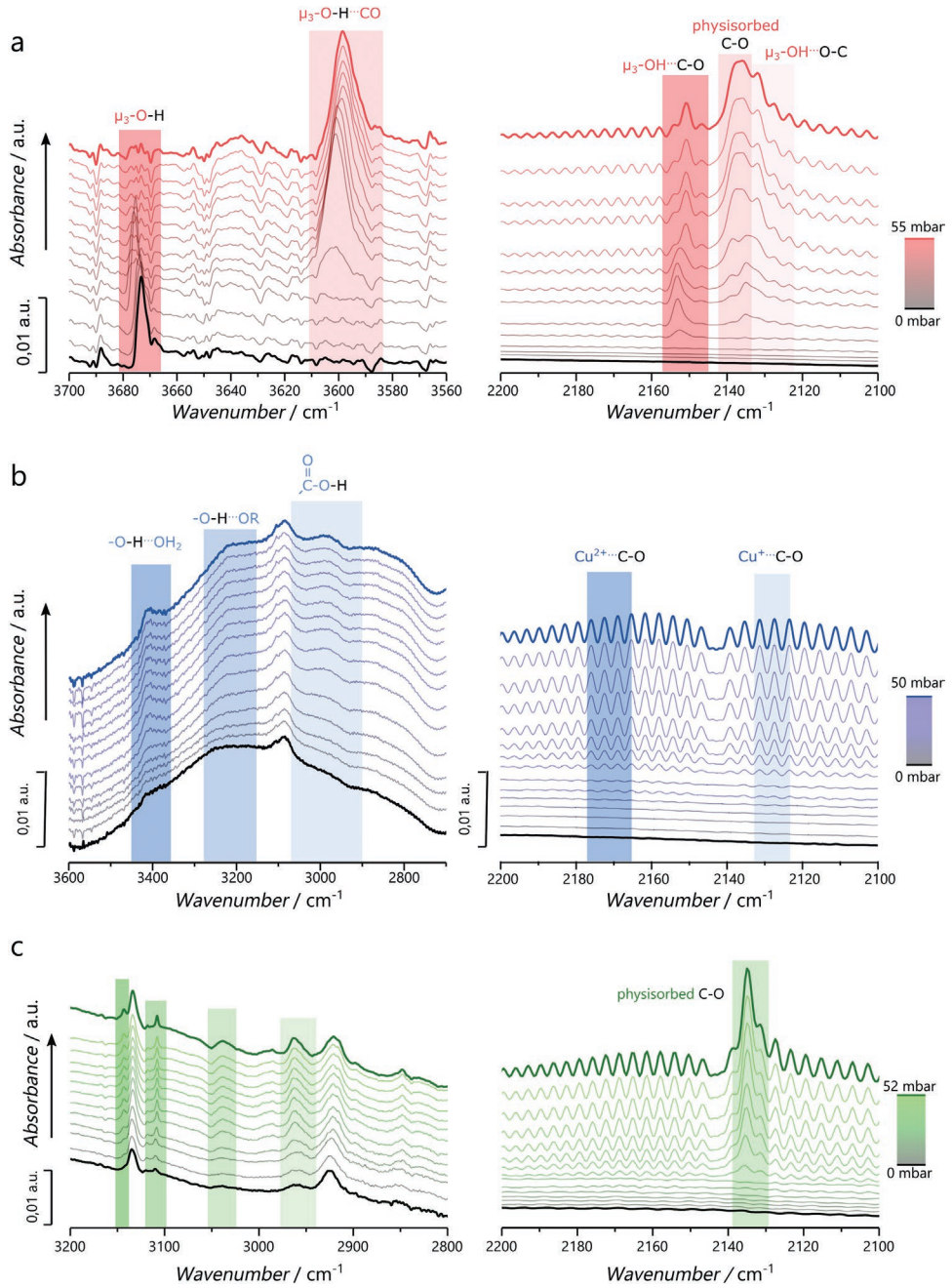

Figure 5. Transmission IR spectra were recorded on a) UiO-67, b) UU-1, and c) ZIF-8 MOF thin films during the adsorption of CO at –188 °C. The left column focusses on the hydrogen-stretching area, revealing the shift of peaks due to their Brønsted acidic nature in UiO-67 and UU-1 for example. The right column focuses on the C—O stretching area, which reveals the bonding of CO on the different MOF sites or as "liquid" confined in the pores.

in between these absorption bands comes from CO in the pores showing "liquid-like" behavior, or is addressed as physisorbed CO.[46,47]

The UU-1 under study consists almost solely of Cu^{2+} in its structure, as demonstrated before by using X-ray photoelectron spectroscopy (XPS), in contrast to its HKUST-1 counterpart, which is known to have very strong redox behavior and often a significant amount of Cu^{+} containing impurities.[11,48,49] After activation, CO is adsorbed and measured in a similar fashion as for UiO-67, as shown in Figure 5b. The OH-region (left) reveals a variety of absorption bands. The hydroxyl groups, which are involved in H-bonding with trapped water molecules and are located around 3400 cm^{-1}, increase in their intensity when CO is adsorbed, as reported before for MIL-53 structures.[50] Two broad bands can be noted with increasing intensity when CO is adsorbed: the band centred around 3200 cm^{-1} and the band centred around 3000 cm^{-1}. Both bands are broad and medium in intensity and undergo a red-shift during CO adsorption. The 3200 cm^{-1} band is attributed to the —OH stretching vibration of intermolecular bonded alcohol groups; thus, is from the linkers

being H-bonded with each other, as known for this structure. The band around 3000 cm^{-1} is due to carboxylic acid groups, so we propose they are due to free linkers. While the alcohol has $\Delta\nu(OH) = -35$ cm^{-1} (3255 to 3220 cm^{-1}), the carboxylic acid group is slightly weaker with $\Delta\nu(OH) = -10$ cm^{-1} (2990 to 2980 cm^{-1}); although, both can be considered as weak acid groups.[42]

The C—O stretching vibrations reveal that only free CO was found, and the only observed modes are the roto-vibrational levels. There are several possible explanations for why expected Cu-adduct bands, for example, 2173 cm^{-1} for Cu^{2+} carbonyls and 2128 cm^{-1} for Cu^{+} carbonyls, are not present.[18,47,51] First of all, we are measuring a thin film material and these adducts might only appear for thicker films due to the low molar amount of adsorbed gas probed amplified by the low concentration of CO adsorbed in general, making it impossible to detect with our current detection limit. Second, this is further complicated by the fact that the UU-1 has approximately half the amount of total Cu sites compared to HKUST-1,[11] and it is suggested that the fibers are very dense; and thus, only the surface Cu-sites will be available.[23,25]

The IR bands formed upon increasing CO pressure for the ZIF-8 material are shown in Figure 5c. In the —H stretching area, two major absorption bands are found for the fresh ZIF-8 material, namely located at 3135 and 2927 cm^{-1}. These bands represent the aromatic and aliphatic C—H stretching vibrations of the 2-methylimidazole linker, respectively.[52] When CO is dosed, the intensities of the two sharp absorption bands at 3144 and 3109 cm^{-1} increase. Furthermore, the intensities of two broad bands located at 3040 and 2960 cm^{-1} increase. As all four bands were already present before CO adsorption, and they are not shifting in position, we believe the increased intensity is not caused by CO adducts.

The CO area shows no distinct sharp bands formed around 2180 cm^{-1}, which would indicate uncoordinated Zn sites or structural defects; hence, demonstrating the low amounts of defects obtained in the applied "flash" synthesis approach.[53] Potential surface Zn-carbonyl species, for example, Zn^{2+} carbonyls at 2225, 2205, and 2155 cm^{-1} or 2100 and 2090 cm^{-1} and Zn^{2+} dicarbonyls at 2205 and 2100 cm^{-1}, were not detected possibly due to the detection limits elaborated on before. Last of all, physisorbed CO similar as observed for UiO-67 was found in the band increase at 2135 cm^{-1}, highlighting the porosity of the sample.

2.6. Interaction With Methanol

Methanol is linked to MOFs in many different ways, for example as solvent, potential catalytic product or as activation agent due to its low surface tension which allows it to "push" water out of the structure. This ability could be utilized even at a larger scale to remove impurities from MOF pores at relatively lower temperatures and in shorter times, making it both practical and cost-wise more efficient than long-term heating at high temperatures. To see if methanol could be used to chemically activate the MOF films in this work, and to study their interaction upon methanol exposure with FT-IR spectroscopy, **Figure 6**a–c shows the IR spectra of UiO-67, UU-1, and ZIF-8 films before and after being exposed to 15 min of liquid methanol, both in ambient conditions and at high vacuum (≈10^{-4} mbar). UiO-67 undergoes a minor but important change in which the μ_3-hydroxyl groups disappear, as the peak at 3675 cm^{-1} is gone after methanol exposure. Furthermore, the carboxylic acid C=O stretch at 1708 cm^{-1} also disappeared which might be due to the removal of remaining unreacted linker or extra-framework linkers or removal of remaining benzoic acid modulator.[16,47] UU-1 changes dramatically after exposure to methanol. The many bands representing unbound

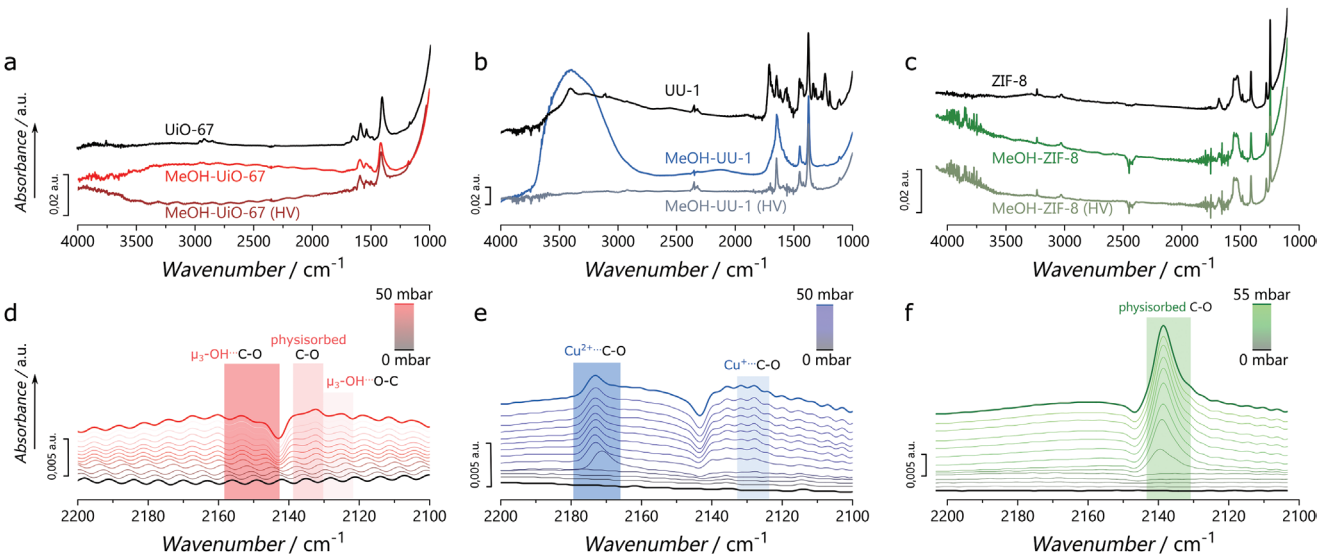

Figure 6. Transmission IR spectra were recorded on a) UiO-67, b) UU-1, and c) ZIF-8 MOF thin films before and after exposure to liquid methanol for 15 min, and after subsequent evacuation to HV (±1.10^{-4} mbar) and activation at 120 °C. d–f) The exposed and evacuated samples were measured during CO adsorption at –188 °C, identical as shown in Figure 5. The methanol quenches UiO-67 bridged hydroxides as they are not available to bind CO. UU-1 undergoes a significant spectral change and after methanol exposure, it has free Cu^{2+} species to bind CO. ZIF-8 seems to be uninfluenced; although, the amount of physisorbed CO increases significantly compared to Figure 5.

carboxylic acid groups, of which it has many, have mostly disappeared.[11] However, the asymmetric and symmetric C—O stretching, typical for Cu-BTC frameworks, remain at 1650 and 1376 cm^{-1}, respectively, and the spectrum is dominated by the presence of water (broad bands at 3700–3000 and 1640 cm^{-1}). This implies that the zigzag-polymers, coordinated by carboxylic acid modulated hydrogen bonds, have been broken. Water is either released from the framework or taken up from the methanol (although present in small amounts) and now physisorbed into the remaining structure, as these bands disappear completely after evacuation revealing a spectrum which closely resembles HKUST-1 (a reference HKUST-1 spectrum is shown in Figure S8, Supporting Information).[15,18,54] For ZIF-8, no major change is observed, which is expected as the ZIF-8 was synthesized in methanol.

To further obtain information on the methanol interaction, CO was probed at –188 °C after activating the methanol exposed MOFs at 120 °C for 1 h and measured with IR, identical as for Figure 5. For UiO-67, Figure 6d confirms that the unbound μ_3 hydroxyls are now unavailable for interaction with CO as the adduct bands are missing completely. This could be due to the formation of methoxy species, which explains why the corresponding O—H stretching band in Figure 6a disappeared. The formation of methoxy species on the Zr nodes is not unknown but often observed on the missing linker sites for UiO-66, while UiO-67 is reported unstable in liquid methanol.[55] On the contrary, in some reports, methanol is the product of CO_2 hydrogenation at elevated temperatures and pressures, and here, intermediate formate species are bound on the missing linker sites instead of the bridged μ_3 hydroxyls.[56] Nevertheless, the dehydration of the bridged hydroxide did show an increase on the formation of methanol and methane in CO_2 hydrogenation and was found to be important in a potential methanol desorption mechanism.[57] Besides the fact that the exposure of these MOFs was at different temperatures and in different forms, it highlights the necessity to understand the interaction of UiO-67 with methanol. The IR spectrum shows no significant change in the vibrations coming from the coordinated linker, and also, the XRD diffractogram of UiO-67 exposed to methanol shows no distinct changes (Figure S9, Supporting Information); thus, it seems the MOF did not fully degrade except for the disappearance of the unbound μ_3 hydroxyl O—H stretching vibration and the unavailability for these sites to bind CO. Therefore, we believe that these sites must have either reacted to form methoxy species or the bridged oxygen bond was broken. However, as practically no CO adduct band was found after the exposure, and this would mean that practically all bridged Zr—OH—Zr bonds would be broken, we assume that the active sites were "poisoned" by methoxy species as the XRD diffractogram shows an intact crystalline structure. Still, activating the MOF in vacuum and at 250 °C did not reverse the effect as there were still no CO adduct bands upon dosing, as seen in Figure S10, Supporting Information. This has large implications for reactions in which the UiO-67 acts as a catalyst as methanol can strongly decrease the availability of the BAS at even higher T and low p.

For UU-1, exposure to methanol revealed IR bands which are commonly found for HKUST-1. In addition, the CO dosing shown in Figure 6e reveals the formation of an adduct band often ascribed to Cu^{2+} species in a paddlewheel formation (marked with the darker blue box). This is again typical for an HKUST-1 species, with contrast to the Cu^{+} species often found in HKUST-1 materials (marked here with the light blue box) and the "liquid"-CO bands being absent. **Figure 7** shows the AFM micrographs and XRD diffractogram of the sample after methanol exposure and surprisingly, it becomes clear that the UU-1 fiber-like morphology has undergone a topotactic transition to HKUST-1 as the AFM shows the morphology containing the typical octahedral crystallites and the XRD pattern reveals the reflections.[10,18,58] This means the UU-1 MOF could act as a precursor to make HKUST-1 SURMOFs with very high initial amounts of Cu^{2+} species, which are often susceptible to redox-behavior.[48]

ZIF-8 was synthesized in methanol and as becomes clear from Figure 6c,f, it did not show a significant change compared to the pristine sample when exposed to methanol. To verify this, Figure S9, Supporting Information, shows the XRD diffractogram after the methanol treatment and the crystalline nature is well preserved. However, the physisorbed CO peak observed in Figure 6f is of higher intensity than observed in Figure 5c: normalized on the ZIF-8 C—N stretching vibration of the linker ≈four times higher. Thus, although we washed the pristine ZIF-8 sample with a methanol flush, we show here that leaving it in methanol for longer times opens even more surface area for the CO to absorb on; and thus, we believe the small remainder of impurities not detected by the method presented here, were even further removed.

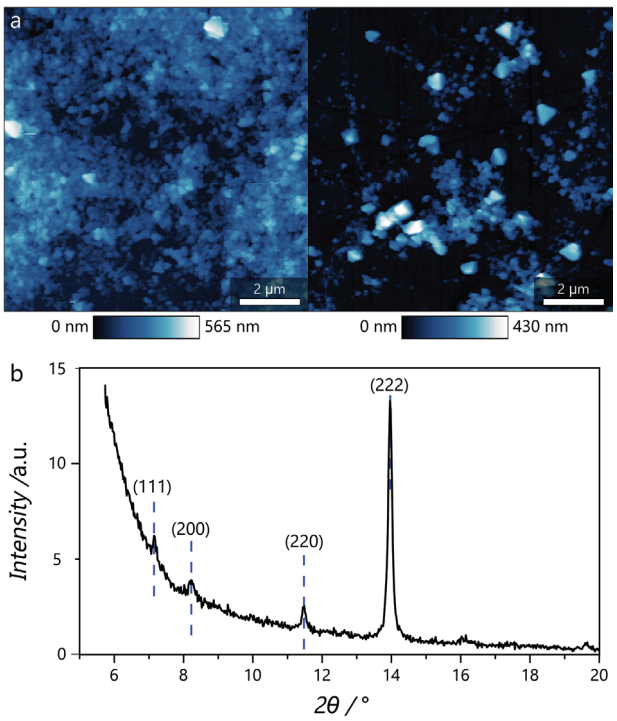

Figure 7. a) Atomic force microscopy (AFM) images showing the UU-1 MOF after exposure to methanol. The long fiber-like web structure as seen in Figure 3 has disappeared, and octahedral crystallites typical, for example, with HKUST-1, are seen. b) XRD indeed reveals the reflections found to be of HKUST-1, meaning the UU-1 has gone through a topotactic transformation upon methanol exposure.

3. Conclusion

We show that CaF_2 windows can anchor a variety of MOFs, including UiO-67, UU-1, and ZIF-8 films. UiO-67 was synthesized using a direct approach; utilizing SEM to visualize this MOF at different time stages in the synthesis procedure, we have observed a Volmer–Weber-based growth mechanism. Smaller anchored crystallites grow to form a film, while in parallel (growing) seeds in the solution anchor on the substrate, which subsequently grows to form a film again, leading to a closed MOF film with increasingly large, exposed crystallite-facet sides over time. We demonstrate the UU-1 to be identical to other reports of Cu-BTC coordination polymers, in which rapid evaporation of the solvents leads to the formation of the $Cu(BTC)(H_2O)_3$ structure instead of the more common HKUST-1 $Cu_2(BTC)_3$ structure. Furthermore, it is demonstrated that the nanoweb structure yields larger micro- and macropores. ZIF-8 was made using a "flash" synthesis, which turned out to follow a Volmer–Weber mechanism. Islands are formed after the initial deposition cycle, and further cycles yield a closed layer and larger growing crystallites. Last, the transparent nature of the CaF_2 windows allow for the spectroscopic investigation of these MOFs with CO probe molecule adsorption FT-IR spectroscopy before and after methanol exposure. With this, the diversity for the MOFs is shown as the methanol "poisoned" the UiO-67 by forming methoxy groups on the bridging hydroxyls, leading to the topotactic transformation of UU-1 into HKUST-1 and did not further influence the ZIF-8; although, it did uncover more surface area due to the removal of impurities. Hence, we show that using CaF_2 windows to allow transmission-based spectroscopic measurements is applicable for a broad range of thin film MOFs made using different synthesis techniques. This can be expanded not only to different (SUR)MOFs but also toward different applications to gain understanding about surface-anchored materials in sensing, separation, catalysis or other physico–chemical processes that can be monitored using (vibrational) spectroscopy.

4. Experimental Section

Materials Synthesis: IR-polished CaF_2 (13 mm × 0.5 mm, supplied by Crystran Ltd, Poole) windows were functionalized with 4-(trifluoromethyl) benzoic acid (98%, Sigma–Aldrich) following the procedure from earlier work.[18] For the UiO-67 MOF, the CaF_2 substrate was directly placed in the mother solution of precursors after functionalization and heated at 100 °C for different durations as indicated in the manuscript. This precursor solution consisted of 2.15 mmol zirconium(IV) chloride (99+%, Sigma–Aldrich) and 2.15 mmol of biphenyl-4,4′-dicarboxylic acid (97%, Sigma–Aldrich), mixed in 0.65 mol of *N*,*N*-dimethylformamide (99.8%, Alfa Aesar) with benzoic acid (21.5 mmol) and hydrochloric acid (1.72 mmol). After this time, the resulting film was washed with DMF and pure ethanol and dried using compressed air. UU-1 was synthesized as described before: an even amount of 10 µM trimesic acid (95%, Sigma–Aldrich) in ethanol (abs, VWR Chemicals) was mixed with 10 µM of $Cu(NO_3)_2$ (99+%, Sigma–Aldrich) in demineralized water and then dropped onto the functionalized CaF_2 window, while rotating at 5000 rpm.[11] The resulting film was washed with ethanol. One layer of material was formed from 0.25 mL of solution, so from a total precursor volume of 10 mL, 400 layers were formed. ZIF-8 was synthesized using a flash-synthesis deposition approach. The CaF_2 substrate was placed on a heating plate at 65 °C. 40 mM of zinc nitrate hexahydrate ($Zn(NO_3)_2 \cdot 6H_2O$) (98%, Sigma–Aldrich) was dissolved in 10 mL of methanol (abs, VWR Chemicals) until a clear solution was obtained. 160 mM of 2-methylimidazole (99%, Sigma–Aldrich) was separately dissolved in 10 mL of methanol to generate another clear solution. For each cycle, 0.2 mL of the metal solution and 0.2 mL of the linker solution were mixed in a separate vial before deposition onto the functionalized CaF_2 window, while constantly heating at 65 °C until the solvents were fully evaporated. In total, six (or less, as indicated in the manuscript) cycles were deposited, and in between each cycle, the resulting film was flushed with methanol and dried with compressed air at room temperature. Bulk HKUST-1 was obtained as Basolite C300 (Sigma–Aldrich).

Materials Characterization: *Scanning Electron Microscopy (SEM)*: SEM micrographs of the MOF films were recorded on a FEI Helios NanoLab G3 UC (FEI Company) instrument coupled with an Oxford Instruments Silicon Drift Detector X-Max energy-dispersive spectroscope. The samples were deposited onto Al stabs with carbon tape (Electron Microscopy Sciences, Hartfield, PA, USA) and coated with 10 nm of Pt. Thereafter, imaging was carried out at a beam of 10 kV and 0.1 nA. Focused ion beam scanning electron microscopy (FIB-SEM) images were taken using the same instrument. Before performing the measurements, a protective layer of Pt was deposited on top of the region of interest. A trench was made by milling perpendicularly to the surface, next to the Pt-deposited area. After milling the trench, a cleaning step was performed before imaging. SEM images of the cross-section were recorded in backscattered mode (2 kV, 0.1nA). Particle/pore size distributions were made using Gwyddion and the "Measure distances" function.[59] The obtained sizes were then plotted using OriginLab and the curves (Lognormal for the PSD in Figure 3, Kernel smooth for the PSD presented in Figure 2) were plotted as a visual representation.

Atomic Force Microscopy (AFM): AFM images were recorded using a Bruker Multimode 8 in non-contact mode with ScanAsyst-Air SiN_3 cantilevers (F = 0.4 N m^{-1}). The acquired data were post-treated using Gwyddion. All micrographs were flattened by a plane background subtraction and alignment of the rows utilizing the "median-of-differences" function. The 3D representations all shared the same physical scales in *x*, *y*, and *z*, and rotational perspective angles, to ensure a fair comparison.

Fourier Transform-Infrared (FT-IR) Spectroscopy: FT-IR spectroscopy during CO adsorption was measured using a PerkinElmer 2000 instrument. The stainless-steel cell contained KBr windows, and measurements were performed using 64 scans, 2 cm^{-1} resolution, and a $LiTaO_3$ detector. Before dosing CO gas, the sample was preheated to 120 °C for 2 h in a vacuum (≈10^{-4} mbar), then cooled down to at −188 °C using liquid nitrogen. The interaction of CO with the MOF films was recorded at increasing pressures due to the dosing of 10% CO/He (v/v) (Linde AG, 99.999%) starting from 0.1 mbar up to 50 mbar. To study the influence of methanol, fresh samples were first put in the cell and a spectrum was recorded. Then, the windows were taken out and put in 1–2 mL of methanol for 15 min. The samples were let to dry in air, then put back into the IR cell. A spectrum was recorded, and the sample was activated as indicated above before CO was dosed in an identical manner.

X-Ray Diffraction (XRD): XRD patterns were collected on a Bruker-AXS D2 Phaser in Bragg–Brentano geometry, using 1 mm Soller slits. A Co Kα radiation (λ = 1.78897 Å) source with 2θ from 5–50° was used with an increment of 0.02° and a step measurement time of 1 s. Data analysis was performed using Eva software.

Supporting Information

Supporting Information is available from the Wiley Online Library or from the author.

Acknowledgements

L.D.B.M. and C.J. contributed equally to this work. This work was supported by The Netherlands Center for Multiscale Catalytic Energy

Conversion (MCEC), an NWO Gravitation program funded by the Ministry of Education, Culture and Science of the government of The Netherlands. This project has received funding from the European Union's Horizon 2020 research and innovation programme under the Marie Skłodowska-Curie grant agreement No 801359.

Conflict of Interest

The authors declare no conflict of interest.

Data Availability Statement

The data that support the findings of this study are available from the corresponding author upon reasonable request.

Keywords

calcium fluoride, film formation, IR spectroscopy, metal–organic frameworks, thin films

Received: August 8, 2022
Revised: October 23, 2022
Published online: December 3, 2022

[1] A. H. Chughtai, N. Ahmad, H. A. Younus, A. Laypkov, F. Verpoort, *Chem. Soc. Rev.* **2015**, *44*, 6804.
[2] O. Shekhah, J. Liu, R. A. Fischer, C. Wöll, *Chem. Soc. Rev.* **2011**, *40*, 1081.
[3] J. Liu, C. Wöll, *Chem. Soc. Rev.* **2017**, *46*, 5730.
[4] V. Stavila, A. A. Talin, M. D. Allendorf, *Chem. Soc. Rev.* **2014**, *43*, 5994.
[5] T. Hashem, E. P. Valadez Sánchez, P. G. Weidler, H. Gliemann, M. H. Alkordi, C. Wöll, *ChemistryOpen* **2020**, *9*, 524.
[6] G. Genesio, J. Maynadié, M. Carboni, D. Meyer, *New J. Chem.* **2017**, *42*, 2351.
[7] B. Liu, O. Shekhah, H. K. Arslan, J. Liu, C. Wöll, R. A. Fischer, *Angew. Chem., Int. Ed.* **2012**, *51*, 807.
[8] L. Yuan, M. Tian, J. Lan, X. Cao, X. Wang, Z. Chai, J. K. Gibson, W. Shi, *Chem. Commun.* **2018**, *54*, 370.
[9] M. Rivera-Torrente, M. Filez, R. Hardian, E. Reynolds, B. Seoane, M. V. Coulet, F. E. Oropeza Palacio, J. P. Hofmann, R. A. Fischer, A. L. Goodwin, P. L. Llewellyn, B. M. Weckhuysen, *Chem. - Eur. J.* **2018**, *24*, 7498.
[10] L. D. B. Mandemaker, M. Filez, G. Delen, H. Tan, X. Zhang, D. Lohse, B. M. Weckhuysen, *J. Phys. Chem. Lett.* **2018**, *9*, 1838.
[11] L. D. B. Mandemaker, M. Rivera-Torrente, G. Delen, J. P. Hofmann, M. Lorenz, A. Belianinov, B. M. Weckhuysen, *Chem. - Eur. J.* **2019**, *26*, 691.
[12] V. Chernikova, O. Shekhah, M. Eddaoudi, *ACS Appl. Mater. Interfaces* **2016**, *8*, 20459.
[13] H. Gliemann, C. Wöll, *Mater. Today* **2012**, *15*, 110.
[14] O. Shekhah, H. Wang, T. Strunskus, P. Cyganik, D. Zacher, R. Fischer, C. Wöll, *Langmuir* **2007**, *23*, 7440.
[15] G. Delen, Z. Ristanović, L. D. B. Mandemaker, B. M. Weckhuysen, *Chem. -Eur. J.* **2018**, *24*, 187.
[16] G. Kaur, S. Øien-Ødegaard, A. Lazzarini, S. M. Chavan, S. Bordiga, K. P. Lillerud, U. Olsbye, *Cryst. Growth Des.* **2019**, *19*, 4246.
[17] S. Øien-Ødegaard, B. Bouchevreau, K. Hylland, L. Wu, R. Blom, C. Grande, U. Olsbye, M. Tilset, K. P. Lillerud, *Inorg. Chem.* **2016**, *55*, 1986.
[18] L. D. B. Mandemaker, M. Rivera-Torrente, R. Geitner, C. M. Vis, B. M. Weckhuysen, *Angew. Chem., Int. Ed.* **2020**, *59*, 19545.
[19] J. Shankwitz, D. Speed, D. Sinanan, G. Szulczewski, *Inorganics* **2021**, *9*, 1.
[20] A. Baskaran, P. Smereka, *J. Appl. Phys.* **2012**, *111*, 044321.
[21] M. L. Ohnsorg, C. K. Beaudoin, M. E. Anderson, *Langmuir* **2015**, *31*, 6114.
[22] M. Wilson, S. N. Barrientos-Palomo, P. C. Stevens, N. L. Mitchell, G. Oswald, C. M. Nagaraja, J. P. S. Badyal, *ACS Appl. Mater. Interfaces* **2018**, *10*, 4057.
[23] J. Gascon, S. Aguado, F. Kapteijn, *Microporous Mesoporous Mater.* **2008**, *113*, 132.
[24] R. Pech, J. Pickardt, *Acta Crystallogr. C* **1988**, *44*, 992.
[25] H. Ahmed, X. Yang, Y. Ehrnst, N. N. Jeorje, S. Marqus, P. C. Sherrell, A. el Ghazaly, J. Rosen, A. R. Rezk, L. Y. Yeo, *Nanoscale Horiz.* **2020**, *5*, 1050.
[26] B. Chen, Z. Yang, Y. Zhu, Y. Xia, *J. Mater. Chem. A* **2014**, *2*, 16811.
[27] S. Tanaka, Y. Tanaka, *ACS Omega* **2019**, *4*, 19905.
[28] A. U. Ortiz, A. P. Freitas, A. Boutin, A. H. Fuchs, F. X. Coudert, *Phys. Chem. Chem. Phys.* **2014**, *16*, 9940.
[29] Z. Wang, A. Bilegsaikhan, R. T. Jerozal, T. A. Pitt, P. J. Milner, *ACS Appl. Mater. Interfaces* **2021**, *13*, 17517.
[30] J. A. Allegretto, J. Dostalek, M. Rafti, B. Menges, O. Azzaroni, W. Knoll, *J. Phys. Chem. A* **2019**, *123*, 1100.
[31] M. J. de Velásquez-Hernández, R. Ricco, F. Carraro, F. T. Limpoco, M. Linares-Moreau, E. Leitner, H. Wiltsche, J. Rattenberger, H. Schröttner, P. Frühwirt, E. M. Stadler, G. Gescheidt, H. Amenitsch, C. J. Doonan, P. Falcaro, *CrystEngComm* **2019**, *21*, 4538.
[32] B. Russell, J. Villaroel, K. Sapag, A. D. Migone, *J. Phys. Chem. C* **2014**, *118*, 28603.
[33] E. P. Valadez Sánchez, A. Knebel, L. I. Sánchez, M. Klumpp, C. Wöll, R. Dittmeyer, *Langmuir* **2020**, *36*, 8444.
[34] H. Zhang, D. Liu, Y. Yao, B. Zhang, Y. S. Lin, *J. Membr. Sci.* **2015**, *485*, 103.
[35] S. Begum, R. R. Haikal, A. H. Ibrahim, M. A. E. Safy, M. Tsotsalas, M. H. Alkordi, *Surf. Interfaces* **2020**, *20*, 100587.
[36] R. D. Deegan, O. Bakajin, T. F. Dupont, G. Huber, S. R. Nagel, T. A. Witten, *Nature* **1997**, *389*, 827.
[37] L.-J. Chen, B. Luo, W.-S. Li, C. Yang, T. Ye, S.-S. Li, X.-Z. Wang, Y.-J. Cui, H.-Y. Li, G.-D. Qian, *RSC Adv.* **2016**, *6*, 7488.
[38] L. Xu, Y. Luo, L. Sun, S. Pu, M. Fang, R. X. Yuan, H. Bin Du, *Dalton Trans.* **2016**, *45*, 8614.
[39] E. M. Thoresen, S. Øien-Ødegaard, G. Kaur, M. Tilset, K. P. Lillerud, M. Amedjkouh, *RSC Adv.* **2020**, *10*, 9052.
[40] S. Goyal, M. S. Shaharun, C. F. Kait, B. Abdullah, *J. Phys.: Conf. Ser.* **2018**, *1123*, 012062.
[41] H. Kaur, G. C. Mohanta, V. Gupta, D. Kukkar, S. Tyagi, *J. Drug Delivery Sci. Technol.* **2017**, *41*, 106.
[42] K. Hadjiivanov, *Identification and Characterization of Surface Hydroxyl Groups by Infrared Spectroscopy*, Elsevier, Amsterdam, The Netherlands **2014**.
[43] M. Rivera-Torrente, L. D. B. Mandemaker, M. Filez, G. Delen, B. Seoane, F. Meirer, B. M. Weckhuysen, *Chem. Soc. Rev.* **2020**, *49*, 6694.
[44] D. M. Driscoll, D. Troya, P. M. Usov, A. J. Maynes, A. J. Morris, J. R. Morris, *J. Phys. Chem. C* **2018**, *122*, 14582.
[45] D. M. Driscoll, D. Troya, P. M. Usov, A. J. Maynes, A. J. Morris, J. R. Morris, *Phys. Chem. Chem. Phys.* **2019**, *21*, 5078.
[46] S. Bordiga, E. E. Platero, C. Otero Areán, C. Lamberti, A. Zecchina, *J. Catal.* **1992**, *137*, 179.
[47] K. I. Hadjiivanov, D. A. Panayotov, M. Y. Mihaylov, E. Z. Ivanova, K. K. Chakarova, S. M. Andonova, N. L. Drenchev, *Chem. Rev.* **2021**, *121*, 1286.
[48] J. Szanyi, M. Daturi, G. Clet, D. R. Baer, C. H. F. Peden, *Phys. Chem. Chem. Phys.* **2012**, *14*, 4383.

[49] W. Wang, D. I. Sharapa, A. Chandresh, A. Nefedov, S. Heißler, L. Heinke, F. Studt, Y. Wang, C. Wöll, *Angew. Chem., Int. Ed.* **2020**, *59*, 10514.
[50] C. Volkringer, T. Loiseau, N. Guillou, G. Férey, E. Elkaïm, A. Vimont, *J. Chem. Soc., Dalton Trans.* **2009**, *53*, 2241.
[51] C. Prestipino, L. Regli, J. G. Vitillo, F. Bonino, A. Damin, C. Lamberti, A. Zecchina, P. L. Solari, K. O. Kongshaug, S. Bordiga, *Chem. Mater.* **2006**, *18*, 1337.
[52] J. G. Vitillo, V. Crocellà, F. Bonino, *Chem. Eng.* **2019**, *3*, 60.
[53] L. H. Wee, T. Lescouet, J. Ethiraj, F. Bonino, R. Vidruk, E. Garrier, D. Packet, S. Bordiga, D. Farrusseng, M. Herskowitz, J. A. Martens, *ChemCatChem* **2013**, *5*, 3562.
[54] S. Bordiga, L. Regli, F. Bonino, E. Groppo, C. Lamberti, B. Xiao, P. S. Wheatley, R. E. Morris, A. Zecchina, *Phys. Chem. Chem. Phys.* **2007**, *9*, 2676.
[55] D. Yang, V. Bernales, T. Islamoglu, O. K. Farha, J. T. Hupp, C. J. Cramer, L. Gagliardi, B. C. Gates, *J. Am. Chem. Soc.* **2016**, *138*, 15189.
[56] E. S. Gutterød, A. Lazzarini, T. Fjermestad, G. Kaur, M. Manzoli, S. Bordiga, S. Svelle, K. P. Lillerud, E. Skúlason, S. Øien-ØDegaard, A. Nova, U. Olsbye, *J. Am. Chem. Soc.* **2020**, *142*, 999.
[57] E. S. Gutterød, S. H. Pulumati, G. Kaur, A. Lazzarini, B. G. Solemsli, A. E. Gunnæs, C. Ahoba-Sam, M. E. Kalyva, J. A. Sannes, S. Svelle, E. Skúlason, A. Nova, U. Olsbye, *J. Am. Chem. Soc.* **2020**, *142*, 17105.
[58] N. Nijem, K. Fürsich, S. T. Kelly, C. Swain, S. R. Leone, M. K. Gilles, *Cryst. Growth Des.* **2015**, *15*, 2948.
[59] D. Nečas, P. Klapetek, *Open Phys.* **2012**, *10*, 181.